ASCE

Shear Strength–Based Determination of the Effective Stress Parameter in Unsaturated Compacted Clayey Soils: Experimental Investigation and Microstructural Interpretation

Hesam Ebrahimisadr[1]; Sophie Lanckohr[2]; and Bertrand François[3]

Downloaded from ascelibrary.org by Bertrand FRANCOIS on 05/02/26. Copyright ASCE. For personal use only; all rights reserved.

Abstract: The χ parameter in the generalized effective stress formulation for unsaturated soils aims at weighting the contribution of suction on the magnitude of effective stress. It is usually expressed as a function of the degree of saturation. This paper presents a comprehensive methodology to calibrate this χ parameter, based on ensuring a unique shear failure criterion when the stresses are represented in terms of generalized effective stress. The method requires knowing the intrinsic strength parameters (effective cohesion and friction angle) from triaxial compression tests upon saturated conditions, and the uniaxial compression strength at various suction levels. The effectiveness of the proposed methodology is verified by applying it to three different compacted clayey soils. Then, the microstructural significance of the obtained relationship between the χ parameter and the degree of saturation is discussed from pore size distribution analyzed from a bimodal perspective. The macroscopic effective stress is primarily governed by the water residing in macropores (interaggregate region), while the water retained within micropores (intra-aggregate region) has a negligible effect on the χ parameter. **DOI: 10.1061/IJGNAI.GMENG-13415**. © *2026 American Society of Civil Engineers*.

Author keywords: Effective stress parameter; Generalized effective stress; Unsaturated soils; Clayey soil; Shear failure criterion; Pore size distribution.

Introduction

Unsaturated soils exhibit complex geomechanical behavior due to the coexistence of two fluid phases in the pore network, leading to pore pressures and surface tensions that affect the global stress–strain response of the material. To consider this three-phase material as an equivalent continuum, the stress definition should encompass the complexity of micromechanics occurring at the pore scale into a macroscopic formulation that models the multiphase porous medium into an equivalent, single-phase, single-stress state continuum (Khalili et al. 2005).

A precise understanding of the macroscopic mechanical behavior of unsaturated soils necessitates a rigorous formulation of the stress state within the medium. Unlike fully saturated conditions, suction, which is an inherent feature of unsaturated soils, directly influences the interparticle contact stresses. As a result, the overall mechanical response of the soil is strongly governed by the prevailing suction level. Therefore, it is essential to incorporate suction, or an appropriate modification of it, to accurately represent the stress state of the material (Gens et al. 2006; Nuth and Laloui 2008). Moreover, the relative proportions of pore air and pore water have a significant influence on the mechanical behavior of unsaturated soils. This ratio, commonly expressed by the degree of saturation, should be considered, either explicitly or implicitly, in any comprehensive description of the soil's hydromechanical state.

According to Terzaghi's (1936) classical concept, effective stress must represent the portion of total stress responsible for all measurable deformations in the soil, including compaction, distortion, and variations in shear resistance. Therefore, the effective stress serves as the fundamental variable governing the elastic and elastoplastic constitutive behavior of the soil skeleton. In other words, the effective stress formulation, combined with an elastoplastic framework, should be able to address the stress–strain response and failure of porous materials under variations in external stress and suction.

Because effective stress formulation requires considering soil suction and relative amounts of the pore air and pore water phases, the water retention curve, which relates suction to the degree of saturation, plays an important role in the geomechanical response of soils. Consequently, suction affects significantly the magnitude of generalized effective stress in clays, because they exhibit high water retention capacity, leading to strong hydromechanical couplings.

In the development and the use of a hydromechanical constitutive model, that aims to describe stress–strain behavior upon varying suction, the consideration of a generalized effective stress framework offers the advantage that all the constitutive equations are expressed as a function of this unique stress variable. However, the complexity stands in the generalized effective stress

[1]Faculty of Applied Sciences, ArGEnCo Dept., Université de Liège, Quartier Polytech Allée de la Découverte, 9—Sart Tilman, 4000 Liège, Belgium. Email: H.Ebrahimisadr@uliege.be

[2]Faculty of Applied Sciences, ArGEnCo Dept., Université de Liège, Quartier Polytech Allée de la Découverte, 9—Sart Tilman, 4000 Liège, Belgium. ORCID: https://orcid.org/0009-0004-5169-5647. Email: Sophie.Lanckohr@uliege.be

[3]Faculty of Applied Sciences, ArGEnCo Dept., Université de Liège, Quartier Polytech Allée de la Découverte, 9—Sart Tilman, 4000 Liège, Belgium (corresponding author). ORCID: https://orcid.org/0000-0001-5075-1222. Email: Bertrand.Francois@uliege.be

Note. This manuscript was submitted on September 18, 2025; approved on February 19, 2026; published online on April 28, 2026. Discussion period open until September 28, 2026; separate discussions must be submitted for individual papers. This paper is part of the ***International Journal of Geomechanics***, © ASCE, ISSN 1532-3641.

formulation, for which the effect of suction must be weighted by a parameter taking into account the relative amount of fluid phases in the pores. Bishop (1959) named this parameter, χ, as the effective stress parameter. Recent experimental studies (Cao and Sun 2025; Haeri et al. 2014, 2023; Likos 2014; Mohyla et al. 2021; Wang et al. 2019) reveal that suction effects on strength and deformation cannot be described by the degree of saturation alone. In their study, Haeri et al. (2014) observed that the yield suction in collapsible loess soils increases with net shear stress ratio under anisotropic conditions, highlighting the need to include initial stress state in the χ calibration process. Zhan et al. (2014) and Wang et al. (2019) further showed that soil deformation during wetting is governed not only by suction but also by anisotropic net stresses, which influence the soil–water retention behavior and collapse potential. These results underscore the importance of developing suction-controlled, anisotropic test procedures for accurate modeling of unsaturated soils (Haeri et al. 2017; Zhou et al. 2014).

Moreover, Zhang and Lu (2020) proposed a unified suction stress concept that decomposes suction into two components: capillary suction stress and adsorptive suction stress. This framework captures the full range of water–particle interactions, offering a better link between suction and the mechanical response in constitutive models (Lu and Likos 2006; Zhang and Lu 2018). The adsorptive contribution, as they argue, becomes dominant at low water contents and should be explicitly considered in defining χ.

In this study, the χ parameter is calibrated specifically for the shear strength failure envelope under controlled suction conditions. The elastoplastic behavior of unsaturated soils is generally governed by two stress variables; however, for the purpose of defining a unique shear failure criterion, a single generalized effective stress formulation is adopted. This approach is therefore based on the shear strength path and does not attempt to generalize χ for other stress paths such as purely elastic loading or wetting-induced collapse, for which additional constitutive components are required to be fully considered.

This approach aligns with the recent discussions in the literature about the (in)definability of effective stress for unsaturated soils. Zhang and Houston (2024) argued that a single effective stress, strictly analogous to Terzaghi's, cannot represent all mechanical responses of unsaturated soils, and therefore its use should be restricted to specific stress paths. Their closure to the subsequent discussions (Zhang and Houston 2025) reinforced this position, emphasizing the risk of misusing the term *effective stress* in the unsaturated soil context. In contrast, Khoshghalb and Shahbodagh (2025) and Morvan and Perić (2025) defended the effective stress framework, showing that with appropriate formulations it can still capture both shear strength and volume change behavior. Rojas (2025) further demonstrated that χ can be defined as a function of the microstructural water distribution, strengthening the needs for experimental calibration.

Building on these contributions, the present work focuses on a shear-based interpretation of the χ parameter, derived from triaxial and uniaxial compression strength (UCS) shear strength tests under controlled suction conditions. The scope of the work is therefore limited to the shear strength behavior of unsaturated soils, without extending to volumetric deformation mechanisms.

Based on the concept of the uniqueness of failure criterion when expressed in effective stress reference, this paper adopts a methodology aiming to calibrate the χ parameter as a power law of the degree of saturation, on three clayey soils with various plasticity indexes. This approach is inspired from the works of Tarantino and El Mountassir (2013), who calibrated the χ parameter on a set of 18 soils (compacted/reconstituted/natural, from sand to clay), and Gerard et al. (2015). It is based on relatively conventional geomechanical laboratory tests (suction control by relative humidity (RH) technique, triaxial compression tests under saturated conditions, and uniaxial compression tests) to provide a straightforward and efficient means to use the effective stress formalism to consider shear strength of unsaturated soils. Then, the paper also proposes a microstructural significance of this χ parameter based on pore size distribution (PSD). This methodology was applied preliminarily by Ebrahimisadr et al. (2025) on a partial set of data. The present study significantly extends that work by including three different compacted clays, additional calibration analyses, and a detailed discussion of the χ–S_r relationship.

The structure of the paper is as follows. The opening section elaborates on the definition and significance of the χ parameter, with different existing formulations according to various authors. Then, the proposed methodology to calibrate the χ parameter is set out. Next, the characteristics of the three tested soils are detailed through their geotechnical properties and the procedure for soil specimen preparation. Subsequently, the experimental techniques employed are detailed, and the results are presented and interpreted within the developed methodology such that the χ parameter can be determined for the three tested soils. Finally, the obtained values are discussed in the light of the soils' microstructure from pore size distributions.

Generalized Effective Stress Framework

Bishop (1959) was the first to propose an extension of Terzaghi's effective stress principle (Terzaghi 1936), originally formulated for saturated soils, to the case of unsaturated porous materials

$$\sigma'_{ij} = \sigma_{ij} + \chi s \delta_{ij} \tag{1}$$

where s = suction; χ = effective stress parameter; σ_{ij} = total stress tensor, representing the externally applied stress; and δ_{ij} = Kronecker symbol, which equals 1 when $i = j$ and 0 otherwise. In this expression, the effective stress parameter of χ changes with the degree of saturation, taking a value of 0 for completely dry soil and 1 under full saturation. This formulation allows a smooth transition between unsaturated and saturated conditions, reducing to Terzaghi's effective stress when $S_r = 1$ (i.e., $\chi = 1$). Numerous authors (Gallipoli et al. 2003, 2018; Khalili and Khabbaz 1998; Öberg and Sällfors 1997; Pham 2022; Zhang and Houston 2024) have explored the correlation between the effective stress parameter χ and the degree of saturation. Their approaches were founded on different criteria, including volumetric deformation and shear strength (Bishop et al. 1960), the comparison of soil behavior under variations in external stress and suction (Jennings and Burland 1962), and the critical state framework (Vanapalli and Fredlund 2000). Recent studies have highlighted the need to incorporate microscale interactions in the effective stress framework. Zhang and Lu (2019) discussed that classical Bishop's χ formulation lacks the capacity to reflect both capillary and adsorptive interactions within the pore network. Lu and Likos (2006) introduced the concept of suction stress as a more comprehensive representation of interparticle forces, combining van der Waals attraction, double-layer repulsion, cementation, capillary tension, and air–water interfacial effects. These forces were shown to contribute significantly to the effective stress even in dry or high-suction states (Lu et al. 2010; Lu and Griffiths 2004). Zhang and Lu (2018) also demonstrated that suction stress depends on both capillary water and adsorptive water, with a proposed formulation involving dual components (adsorptive and capillary suction

Downloaded from ascelibrary.org by Bertrand FRANCOIS on 05/02/26. Copyright ASCE. For personal use only; all rights reserved.

stress), providing a physical interpretation for χ based on water content and pore structure (Zhang and Lu 2020).

Numerous studies have proposed alternative expressions linking the χ parameter to the degree of saturation or soil suction, or a modified version of them, and eventually some microstructural features. The Appendix reports some of those expressions.

Nikooee et al. (2013) and Gray et al. (2009) include the effect of surface tension at the air–water interface. However, this information is usually not available from conventional experimental characterization. The expression

$$\chi = \frac{S_r - S_r^m}{1 - S_r^m} \tag{2}$$

originally proposed by (Tarantino and Tombolato 2005) and subsequently adapted by Alonso et al. (2013), Vaunat and Casini (2017), and Alonso et al. (2010), includes the pore size distributions as a key factor to calibrate the χ parameter. Here, S_r^m represents the microstructural degree of saturation, corresponding to the degree of saturation required to fill the microporosity, while the macroporosity remains dry. In this concept, the ratio between microporosity and total porosity governs the evolution of χ with the degree of saturation. At low degrees of saturation, water is primarily retained within the aggregates, and this intra-aggregate water does not contribute to the macroscopic stress (i.e., χ remains negligible). However, as the degree of saturation increases, water progressively invades the interaggregate voids, thereby contributing to a greater rise in the internal stress; consequently, the χ parameter becomes more significant. This approach is especially suitable for dual-structured materials that exhibit two distinct pore size domains, larger pores located between aggregates and smaller ones contained within the aggregates. Following this idea, the power–law relationship with the degree of saturation is expressed in the following equation:

$$\chi = (S_r)^{\alpha} \tag{3}$$

with an α exponent higher than 1, proposed by Alonso et al. (2010), making the χ parameter increase slowly upon a low degree of saturation, whereas the rate of increase becomes more pronounced as the degree of saturation rises. So, the α exponent is related to the ratio between microporosity and total porosity. A high value of α exponent corresponds to a soil that has a large ratio of microporosity considering the total porosity, such that the water stored in this microporosity does not contribute to the interaggregate skeleton stress (i.e., the generalized effective stress). This concept is illustrated in Fig. 1, where Eqs. (2) and (3) are compared.

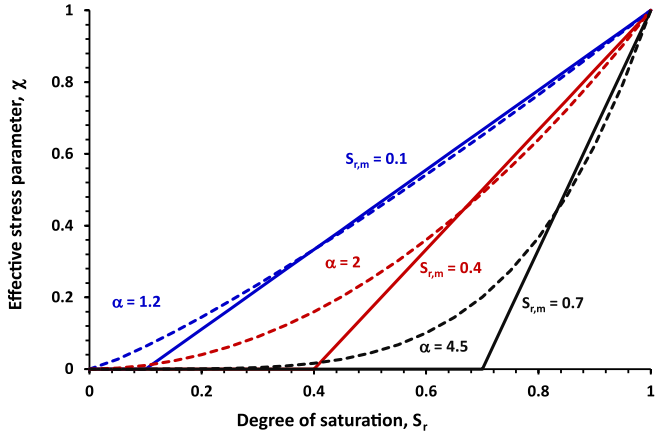

Fig. 1. Comprehensive justification of the χ parameter evolving as a power law of the degree of saturation, based on microstructural features, according to Alonso et al. (2010).

Methodology for χ Parameter Calibration

The objective of developing equations for effective stress in unsaturated soils is to derive a formulation of the generalized effective stress that ensures a unique failure criterion. This failure criterion should not be influenced by suction and the degree of saturation when represented in terms of effective stress (Gerard et al. 2015). Combining generalized effective stress formulation [Eq. (1)] with the conventional Mohr–Coulomb shear failure criterion reveals that the effect of suction and degree of saturation on the shear resistance is indirectly considered through the χ parameter

$$\begin{aligned} \tau_f &= c + \sigma'_N \tan\phi \\ &= c + (\sigma_N + \chi s)\tan\phi \\ &= c + \chi s \tan\phi + \sigma_N \tan\phi \end{aligned} \tag{4}$$

where c = cohesion; ϕ = friction angle; σ'_N = effective normal stress; σ_N = total normal stress; and τ_f = shear stress at failure.

Accordingly, the term $\chi s \tan\phi$ can be considered an additional strength provided by soil suction, usually called capillary cohesion. In other words, the product χs plays a similar role to external normal stress. It exerts internal stress within a soil specimen, even in the absence of any external stress. This internal stress depends on the water conditions of the sample, which are expressed through the product of the effective stress parameter and suction. So, suction can be considered as an internal confining stress. Externally unconfined specimens can be regarded as internally confined once the stress state is expressed within the effective stress framework. The stress state expressed in generalized effective stress can be represented on a Mohr circle diagram by shifting the Mohr circles plotted in terms of total stress to the right by an amount equivalent to χs (Fig. 2) (Gerard et al. 2015).

When starting from uniaxial compression strength under different suction levels, the calibration of the χ parameters requires finding an appropriate expression for χ as a function of the degree of saturation (or eventually suction), which allows horizontal shifting of the Mohr circles obtained at failure so that they align with the failure criterion defined in terms of effective stress. The horizontal offset between the Mohr circle plotted in terms of total stress and

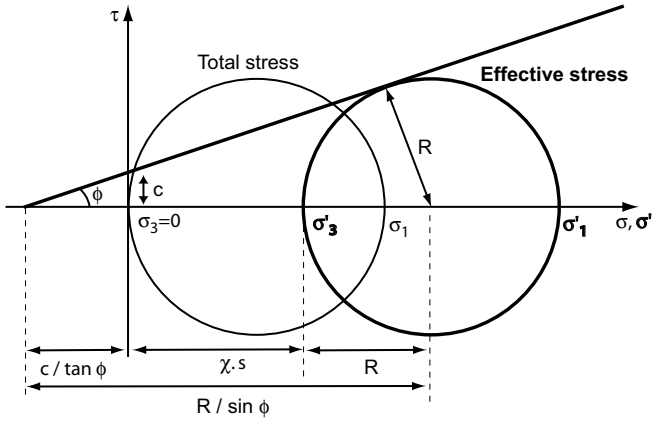

Fig. 2. Mohr circles corresponding to stress state at failure upon uniaxial compression expressed in terms of total stress and generalized effective stress. (Adapted from Gerard et al. 2015.)

Downloaded from ascelibrary.org by Bertrand FRANCOIS on 05/02/26. Copyright ASCE. For personal use only; all rights reserved.

the corresponding failure envelope corresponds to the product χs and can be obtained through a geometric relationship based on stresses and intrinsic parameters, as illustrated in Fig. 2.

The value of the effective stress parameter is then given by the following equation (Gerard et al. 2015):

$$\chi = \frac{\frac{R - c\cos\phi}{\sin\phi} - R}{s} \tag{5}$$

where R = radius of the Mohr circle, defined as $R = (\sigma_1 - \sigma_3)/2$. For uniaxial compression tests, no external stress is applied leading to $\sigma_3 = 0$.

Considering the power law of the degree of saturation [Eq. (3)] expressed in a double logarithmic plane in

$$\log\chi = \alpha \log S_r \tag{6}$$

the α exponent is a material-dependent parameter that corresponds to the slope of the regression line in the ($\log S_r$;$\log\chi$) plane.

For each test result, corresponding to a specific suction and degree of saturation, a single χ value can be determined. Consequently, a series of data points can be plotted in the ($\log S_r$;$\log\chi$) space, from which the best-fitting regression line is obtained, with its slope representing the α parameter.

The complete methodology involves conducting shear tests, either triaxial compression or direct shear tests, under saturated conditions to establish the intrinsic effective shear strength criterion, defined by the effective cohesion and friction angle. Subsequently, a series of uniaxial compression tests performed at different suctions (corresponding to varying degrees of saturation) are used to determine a single χ value for each S_r. At the end, the α exponent is calibrated to find the best fit between Eq. (3) and $\chi(S_r)$.

Table 1. Physical parameters of the three tested soils

Soil	Soignies	Kruibeke	Tournai
Liquid limit (%)	36.4	56	141.1
Plastic limit (%)	18.6	29.7	42.76
Shrinkage limit (%)	9	14.4	27
Plasticity index (%)	17.8	26.3	98.3
Soil type (USCS)	CL	CH	CH
Maximum dry unit weight under standard proctor condition (g/cm^3)	1.72	1.45	1.04
Optimum water content under standard proctor compaction (%)	18	27	47.6
Initial degree of saturation in the as-compacted state (%)	87	81	85
Matric suction in the as-compacted state[a] (MPa)	0.785	1.67	1.063
Total suction in the as-compacted state[a] (MPa)	1.291	2.104	1.351

[a]Measured using the filter paper method in accordance with ASTM D5298-10 (ASTM 2010).

Materials and Methods

Material Properties

Three types of compacted clayey soils were investigated in this study, namely, "Soignies," "Kruibeke," and "Tournai," which are named after the Belgian sites from which they were extracted. These three soils exhibit different characteristics to cover a range of soil behaviors from silt to clay. To characterize the materials, particle size distribution tests, Atterberg limit determination, and standard Proctor compaction tests were performed. The results are reported in Table 1. Matric and total suctions of the soils under as-compacted state were measured in accordance with accordance with ASTM D5298-10 (ASTM 2010). Table 2 reports the mineralogical composition of the tested soils, focusing exclusively on the clay minerals.

According to the particle size distribution curves (Fig. 3), a significant portion of the soil particles have a diameter smaller than 80 μm. This fraction represents 85.6% for the Soignies soil, 83.7% for the Kruibeke soil, and 88.5% for the Tournai soil. Their grain size distribution is relatively similar, but they exhibit different geomechanical properties due to different mineralogical compositions. In particular, Tournai soil is very plastic (I_p = 98.3%) because of the presence of the illite–smectite mixed layer (Table 2). According to the Unified Soil Classification System (USCS), the soil from Soignies corresponds to low plasticity clay (CL), whereas the soils from Kruibeke and Tournai correspond to high plasticity clay (CH).

Sample Preparation

The soil samples were prepared by static compaction at the optimum conditions obtained from the Standard Proctor test, in terms of water content and dry density. Initially, the soil was mixed with the required amount of water to achieve the optimum water content. Then, the wet soil was left to rest for at least 24 h in a plastic bucket to ensure uniform water distribution throughout the soil. To prevent any moisture loss, a plastic film was placed between the lid and the bucket. The bucket was then inverted to rest on its lid to further minimize potential water loss. Finally, the samples were prepared by compacting the soil into a cylindrical mold (see the dimensions in Table 3). The mass of soil inserted into the mold was adjusted to correspond to the optimum Standard Proctor density. All samples were compacted from top to bottom. The specimens were compacted statically in three layers (except for the small specimens used for the water retention curve, which were compacted in a single layer) using a hydraulic jack.

Methods

The saline-solution method was employed to impose different RH levels, thereby generating corresponding suction values, as described by Delage et al. (1998). This technique enables the application of suctions ranging from 4.2 MPa (RH = 0.97) to 59.4 MPa (RH = 0.65), while the laboratory conditions imposed a higher suction of

Table 2. Mineralogical composition of the tested soils, focusing on clay minerals

Soil	Illite (%)	Illite–chlorite mixed layer (%)	Illite–smectite mixed layer (%)	Smectite (%)	Kaolinite (%)	Chlorite (%)	Total clay mineral (%)
Soignies	17	8	8	3	10	5	52
Kruibeke	17	11	10	3	8	12	61
Tournai	10	5	44	6	—	—	65

Source: Data from Schmitz et al. (2004).

Downloaded from ascelibrary.org by Bertrand FRANCOIS on 05/02/26. Copyright ASCE. For personal use only; all rights reserved.

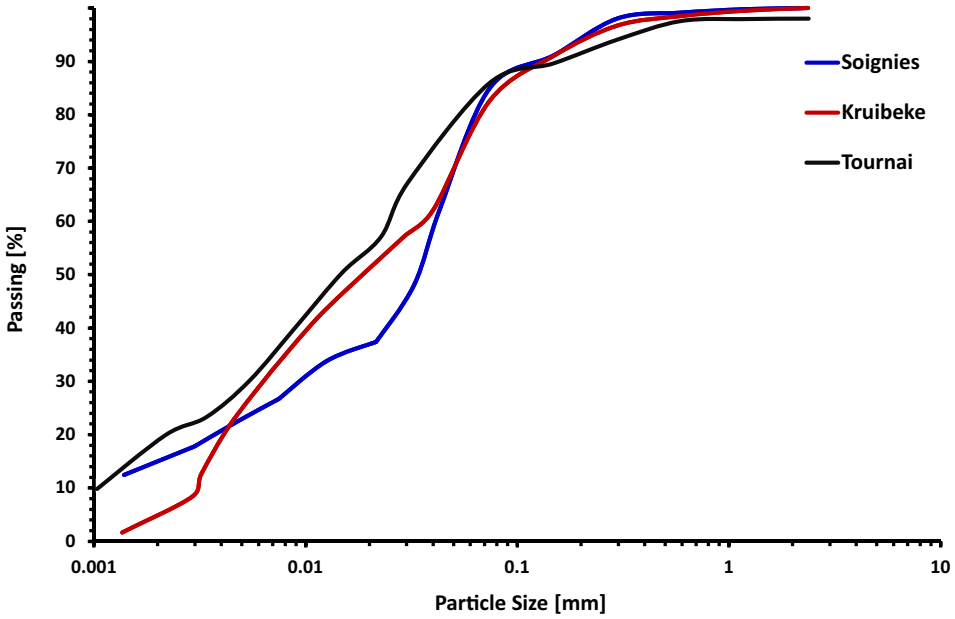

Fig. 3. Particle size distribution curve for the three tested soils.

Table 3. Dimensions of the samples for each test

Test	WRC	UCS	Triax CU
Height (mm)	7.5	50	99
Diameter (mm)	33.2	25	51

Note: WRC = water retention curve; UCS = uniaxial compression test; and Triax CU = Consolidated undrained triaxial test.

110 MPa (RH = 0.45). The dimensions of the cylindrical specimen were measured with a caliper, after compaction and after reaching hydric equilibrium, to evaluate the deformation upon drying.

Furthermore, the mass was measured after compaction, after reaching hydric equilibrium, and after complete drying in an oven at 105°C, to determine the water content and degree of saturation and to construct the water retention curve.

Additionally, as an alternative, the water retention capacity of the three tested soils was determined from dynamic vapor sorption (DVS) (Arlabosse et al. 2003) on small soil fragments (less than 1 cm in size) by recording equilibrium mass values at each humidity step. With this technique, the applied suction ranges from 14 to 670 MPa. However, because the volume variation of the soil fragments during drying was not measured, the degree of saturation could not be deduced and the water retention curve could only be plotted in terms of water content.

Then, the water retention curve was fitted using the van Genuchten (1980) model as follows:

$$S_r = \left[1 + \left(\frac{s}{P_r}\right)^n\right]^{((1/n)-1)} \tag{7}$$

where P_r and n are fitting parameters associated with the material. The curve is calibrated using the experimental points to achieve the best match, as determined by the least squares method.

Triaxial compression tests were performed on saturated soil specimens under consolidated (CU) undrained conditions, with the measurement of pore-water pressure to allow for the deduction of intrinsic shear failure criterion (i.e., effective cohesion and friction angle). Confining pressures of 100, 200, and 400 kPa were imposed.

Uniaxial compression tests were conducted at a loading rate of 0.3 mm/min on specimens subjected to six suction levels (five controlled relative humidity conditions and one under laboratory atmosphere). For each test, the elastic stiffness was determined as the maximum slope of the axial stress–axial strain curve within an axial strain interval of 0.2%. In contrast, the uniaxial compressive strength (UCS) was defined as the peak axial stress attained on the curve.

Experimental Results

Triaxial Tests (CU)

The results of consolidated undrained triaxial compression tests are illustrated in Figs. 4–6, showing the variations of deviatoric stress q with axial strain ε_1, water pressure u_w with axial strain ε_1, and the deviatoric stress q with mean effective stress p' for the three investigated soils. Mohr circles at failure are also plotted together with the deduced failure criterion. The data reflect the behavior of soil samples under confining pressures of 100, 200, and 400 kPa.

The failure criterion was defined as the condition corresponding to the maximum axial stress (σ_1 maximum). From these results, effective cohesion c and the friction angle ϕ have been deduced as summarized in Table 4.

Water Retention Curves

Fig. 7 reports the water retention curves concerning water content [Fig. 7(a)] and degree of saturation [Fig. 7(b)]. The experimental points obtained from the DVS technique are only reported as water content because the volume variation of the specimen upon drying was not measured, so the degree of saturation could not be deduced. The fitting curve, according to the van Genuchten equation, adapts well to the experimental results. Table 5 reports the van Genuchten calibration parameters for the three tested soils. The slope of the curve of the Tournai soil is much lower than that of the Soignies or Kruibeke soil, which appears similar, revealing a higher water retention capacity of the Tournai soil.

Downloaded from ascelibrary.org by Bertrand FRANCOIS on 05/02/26. Copyright ASCE. For personal use only; all rights reserved.

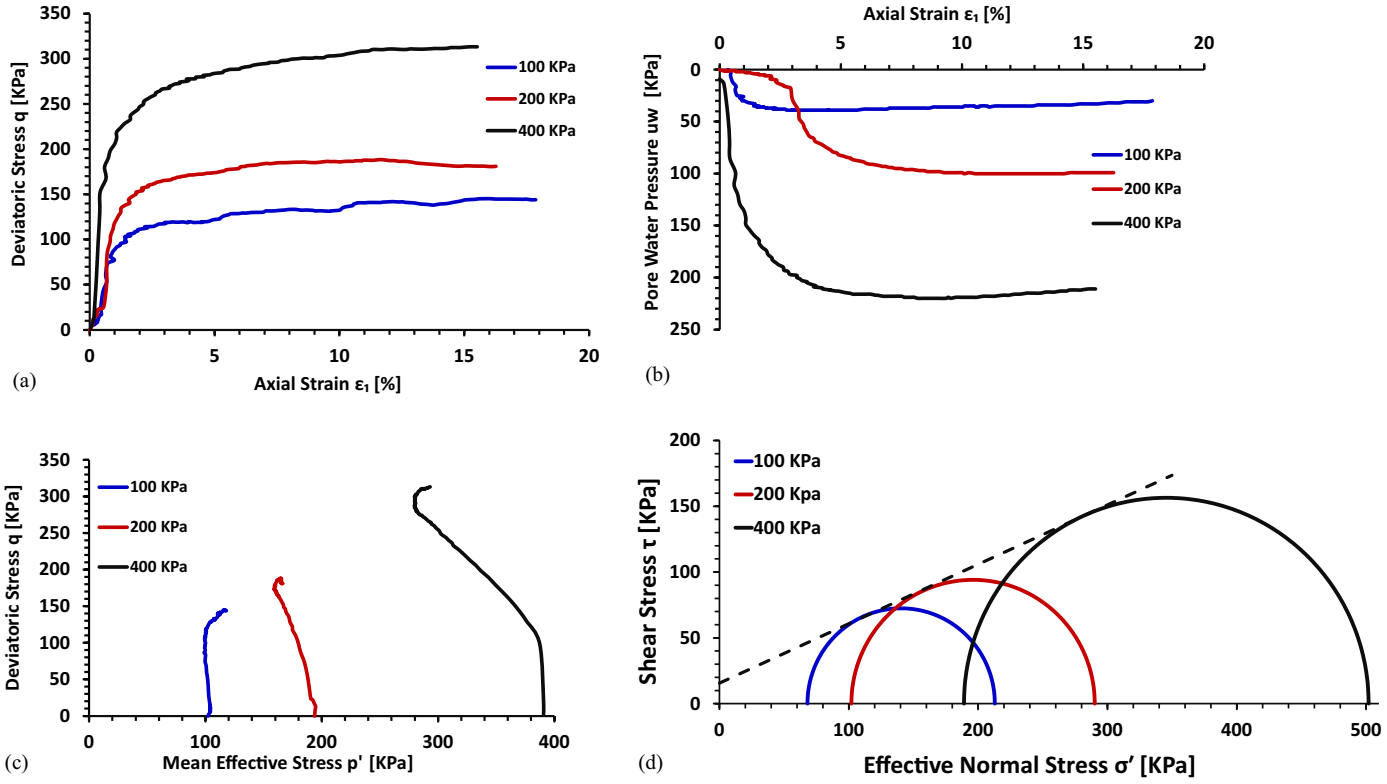

Fig. 4. Results of CU triaxial compression test on Soignies soil upon saturated conditions: (a) deviatoric stress versus axial strain; (b) pore-water pressure versus axial strain; (c) stress paths in $p'-q$ space; and (d) stress state at failure through Mohr circle representation.

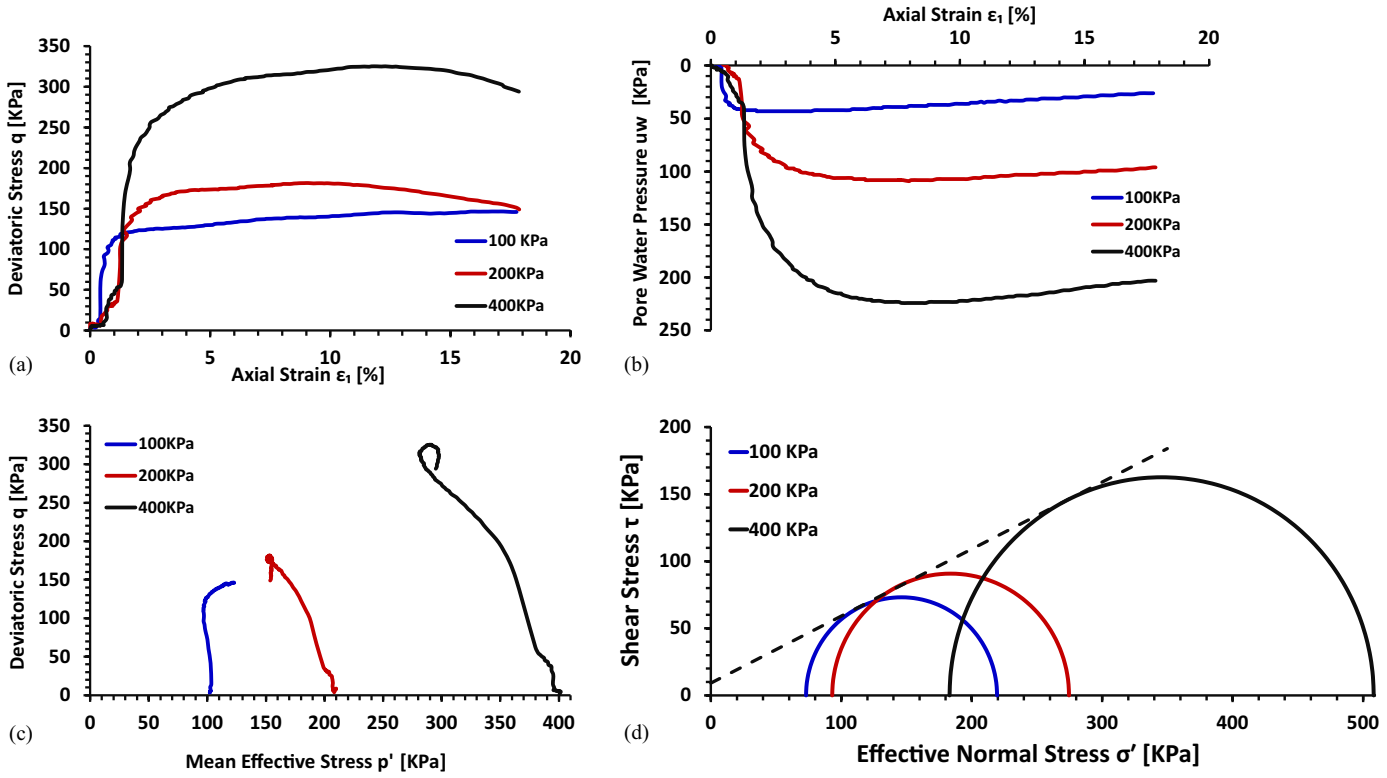

Fig. 5. Results of CU triaxial compression test on Kruibeke soil upon saturated conditions: (a) deviatoric stress versus axial strain; (b) pore-water pressure versus axial strain; (c) stress paths in $p'-q$ space; and (d) stress state at failure through Mohr circle representation.

Downloaded from ascelibrary.org by Bertrand FRANCOIS on 05/02/26. Copyright ASCE. For personal use only; all rights reserved.

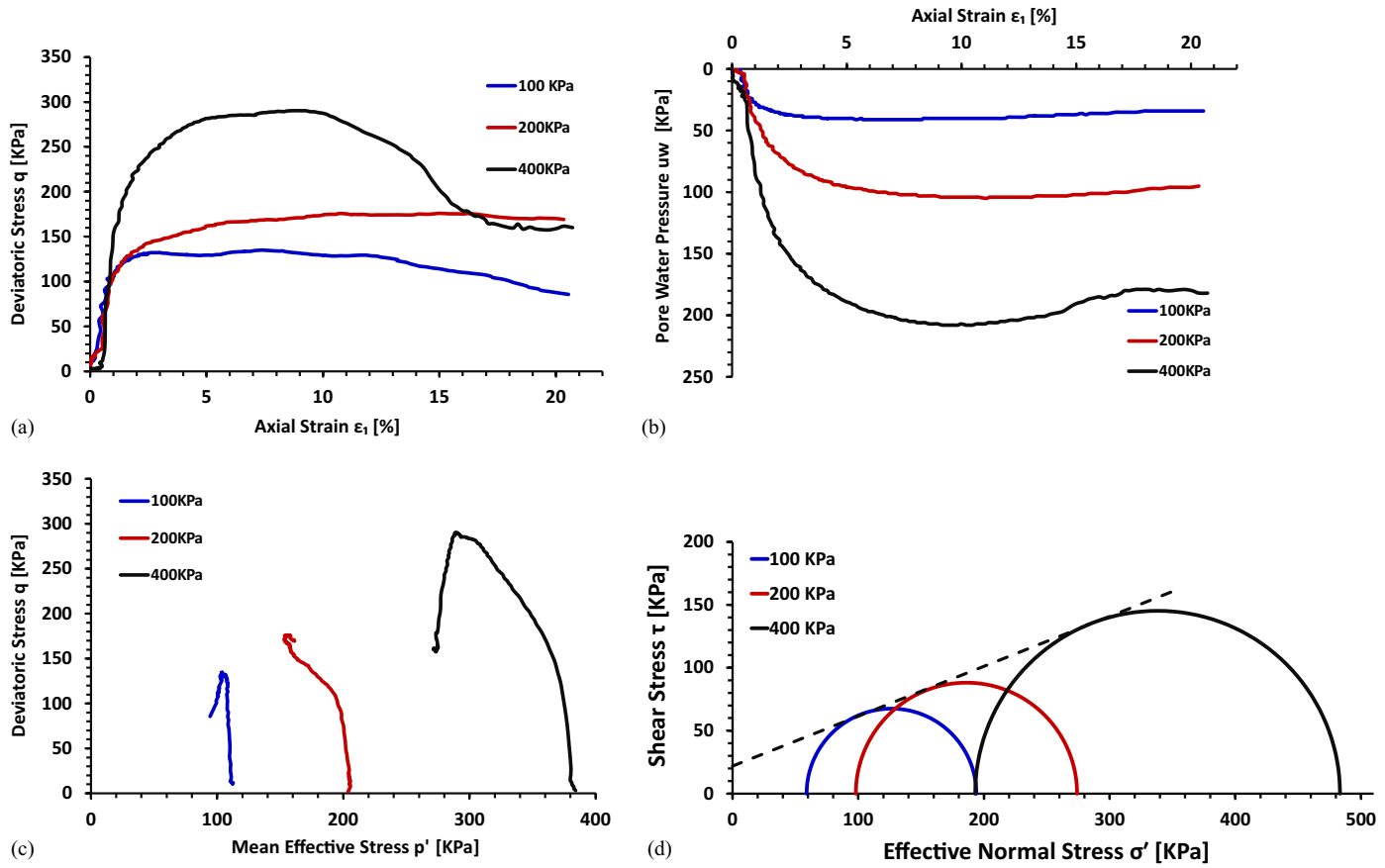

Fig. 6. Results of CU triaxial compression test on Tournai soil upon saturated conditions: (a) deviatoric stress versus axial strain; (b) pore-water pressure versus axial strain; (c) stress paths in $p'-q$ space; and (d) stress state at failure through Mohr circle representation.

Table 4. Effective cohesion and friction angle derived from CU triaxial compression tests performed under saturated conditions

Soil	c (kPa)	ϕ (degrees)
Soignies	15.5	24.3
Kruibeke	9.2	26.6
Tournai	21.8	21.6

This is consistent with the higher plasticity index of the Tournai soil compared with the Soignies and Kruibeke soils.

Volumetric Strain

The volumetric deformation corresponding to each applied suction is reported in Fig. 8 for the three soils. Every reported point being taken on a different specimen may explain the relative variability of the obtained points. The three soils initially undergo significant shrinkage during drying at a relatively low suction level, followed by less or nearly no shrinkage during drying at the higher suction level. This is due to the progressive densification of the material upon drying that induces a stiffening leading to less shrinkage propensity. The Tournai soil exhibits the largest volumetric strain upon drying, due to its high initial water content and low dry density, leading to significant shrinkage upon drying.

Uniaxial Compression Test

Fig. 9 presents the axial stress–axial strain curves for the three soils tested under uniaxial compression at various suction levels, ranging from 4.2 to 110 MPa. Based on these results, Young's modulus and UCS are plotted as function of suction in Fig. 10.

Calibration of the χ Parameter

According to the methodology exposed in the "Methodology for χ Parameter Calibration" section, the relationship between the χ parameter and the degree of saturation can be established by calibrating the exponent in Eq. (3). The underlying principle is to ensure the uniqueness of the shear failure criterion, regardless of the suction level, when the stress state is expressed in terms of the generalized effective stress. According to Eq. (6), α is the slope of the (log S_r;logχ) linear regression curve passing through the origin of the graph (because when $S_r = 1$, $\chi = 1$, i.e., when log $S_r = 0$, log$\chi = 0$).

To evaluate the influence of experimental uncertainties in the UCS on the calibration of the χ parameter, a sensitivity analysis was performed.

In addition to the measured UCS value, two additional calibration curves were constructed by considering $\pm 10\%$ variation in UCS strength. Fig. 11 illustrates these three calibration curves for each soil. The results show that the $\pm 10\%$ variation in UCS induces only a minor shift in the χ–S_r relationship, confirming the robustness of the proposed calibration approach with respect to possible experimental errors in UCS testing.

As shown in Fig. 11, the best fit is obtained for $\alpha = 2.20$ for Soignies soil, $\alpha = 2.62$ for Kruibeke soil, and $\alpha = 3.97$ for Tournai soil.

The results of the uniaxial compression tests conducted under different suction levels are illustrated in Fig. 12 as Mohr circles plotted within the generalized effective stress framework for the three investigated soils. It can be observed that, consistent with the concept underlying the proposed calibration method, the failure envelopes defined by these circles tend to merge into a single

Downloaded from ascelibrary.org by Bertrand FRANCOIS on 05/02/26. Copyright ASCE. For personal use only; all rights reserved.

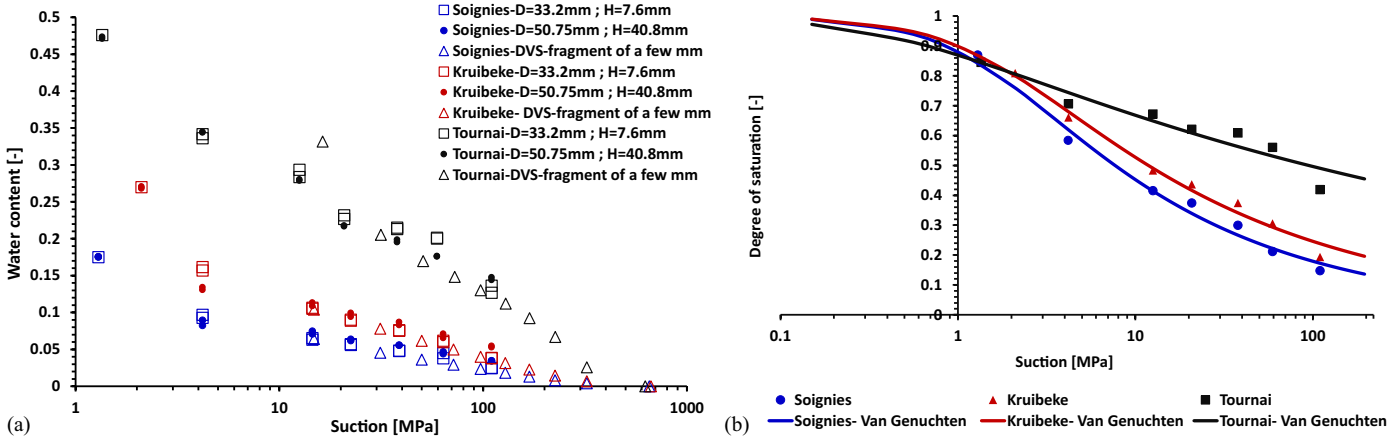

Fig. 7. Water retention curve of the three soils in terms of (a) water content versus suction; and (b) degree of saturation versus suction.

Table 5. Calibration parameters (P_r and n) derived from the van Genuchten model

Soil	P_r (MPa)	n
Soignies	1.51872	1.410
Kruibeke	1.62026	1.34
Tournai	0.46177	1.130

criterion governed by the effective cohesion and friction angle obtained from saturated triaxial tests. Even if the alignment is not perfect, it corresponds to the best fit in Fig. 11.

Microstructural Interpretation

The variation of the effective stress parameter χ in unsaturated soils is intrinsically associated with the microstructural transformations that take place within the pore network. Based on the framework proposed by Tarantino and Tombolato (2005), subsequently adapted by Alonso et al. (2010), Alonso et al. (2013), and Vaunat and Casini (2017), only the water occupying the interaggregate or macropore spaces contributes to the macroscopic effective stress, whereas the water retained within intra-aggregate or micropores does not influence the χ parameter [Eq. (2) and Fig. 1]. When the water remains confined inside the aggregates, χ stays constant. Once the aggregates reach full saturation, any additional water infiltrates the larger voids, generating capillary interactions between aggregates that consequently increase the value of χ.

Consequently, the PSD serves as a reliable indicator of the relationship between the χ parameter and the degree of saturation. Fig. 13 illustrates the PSDs of the three investigated soils in their initial state, prior to any suction application, as determined by mercury intrusion porosimetry (MIP). The boundary between micro- and macroporosity is identified at the minimum point of the PSD curve, corresponding to an intermediate pore diameter. The cumulative volume of intruded mercury for voids larger than this threshold is the macrovoids while the cumulative volume for smaller voids is the microvoids. On that basis, the macro- and microporosity, as obtained from MIP are reported in Table 6. The total porosity, as determined from external volumes and dry masses, is slightly higher than the total intruded porosity. The difference between total porosity and intruded porosity is attributed to the microporosity because it is considered to correspond to very small

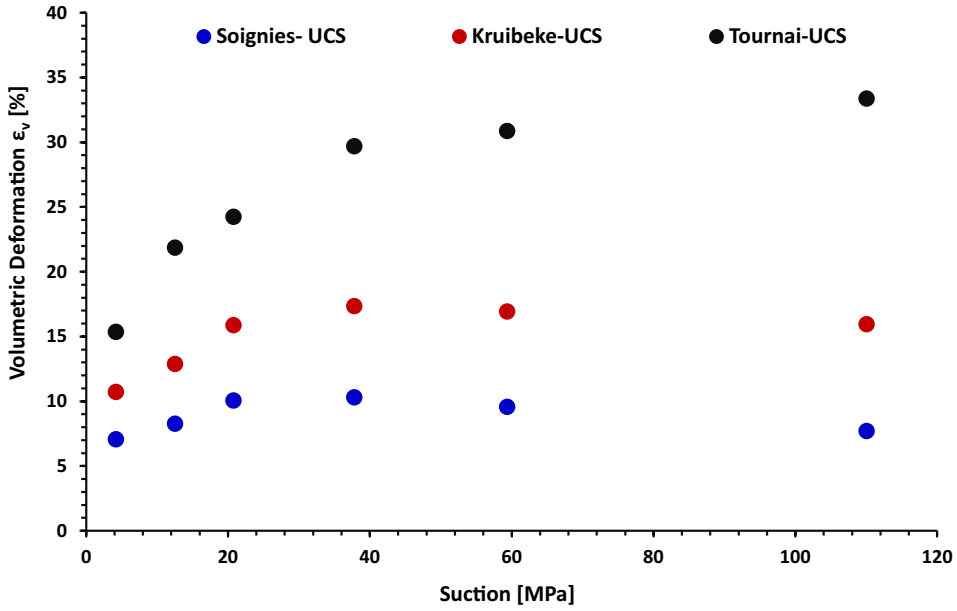

Fig. 8. Volumetric deformations upon drying as a function of suction.

Downloaded from ascelibrary.org by Bertrand FRANCOIS on 05/02/26. Copyright ASCE. For personal use only; all rights reserved.

Downloaded from ascelibrary.org by Bertrand FRANCOIS on 05/02/26. Copyright ASCE. For personal use only; all rights reserved.

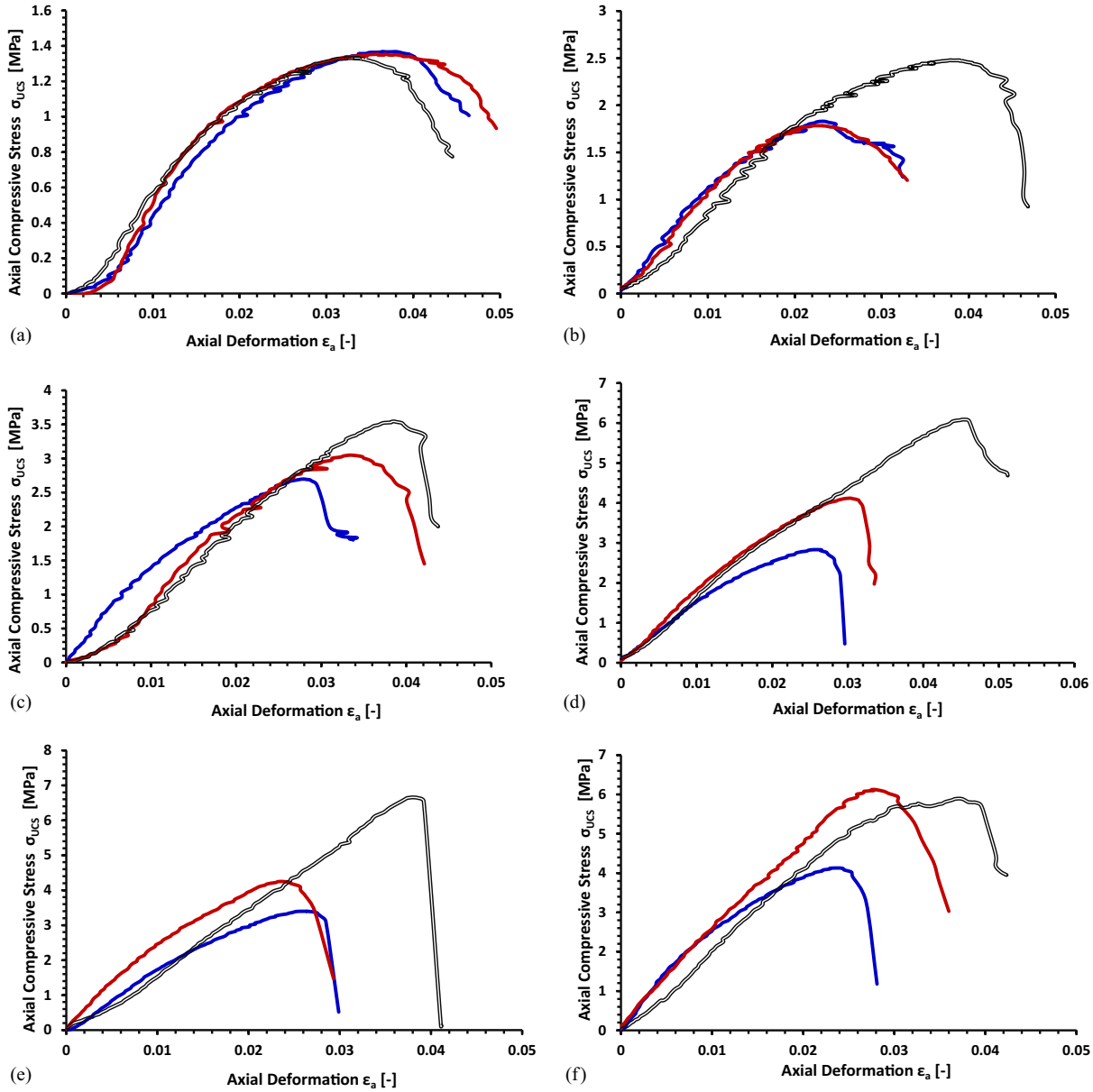

Fig. 9. Results of uniaxial compression tests at various suction levels: (a) $s = 4.2$ MPa; (b) $s = 12.55$ MPa; (c) $s = 20.8$ MPa; (d) $s = 37.8$ MPa; (e) $s = 59.4$ MPa; and (f) $s = 110.1$ MPa.

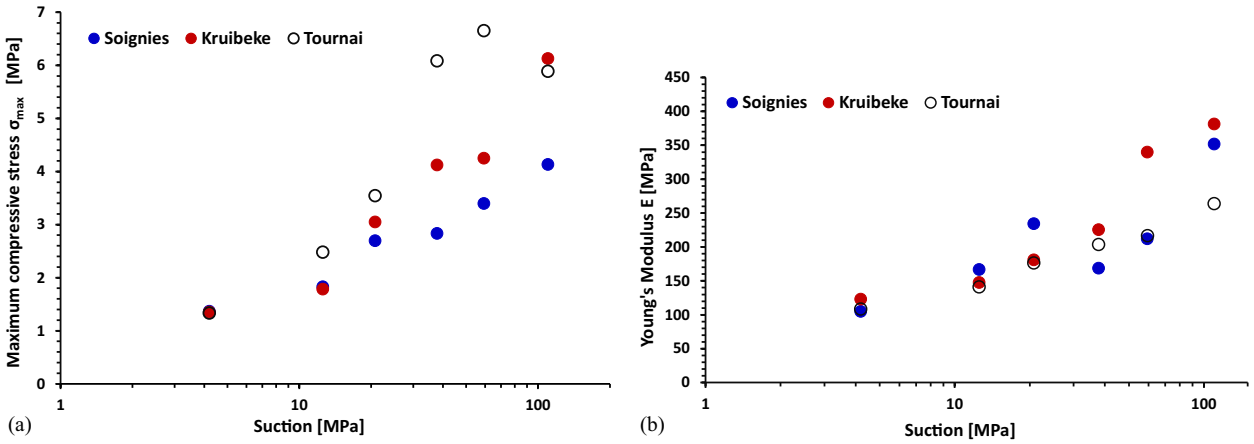

Fig. 10. Evolution of (a) uniaxial compressive strength; and (b) Young's modulus experienced during uniaxial compression tests, as a function of suction.

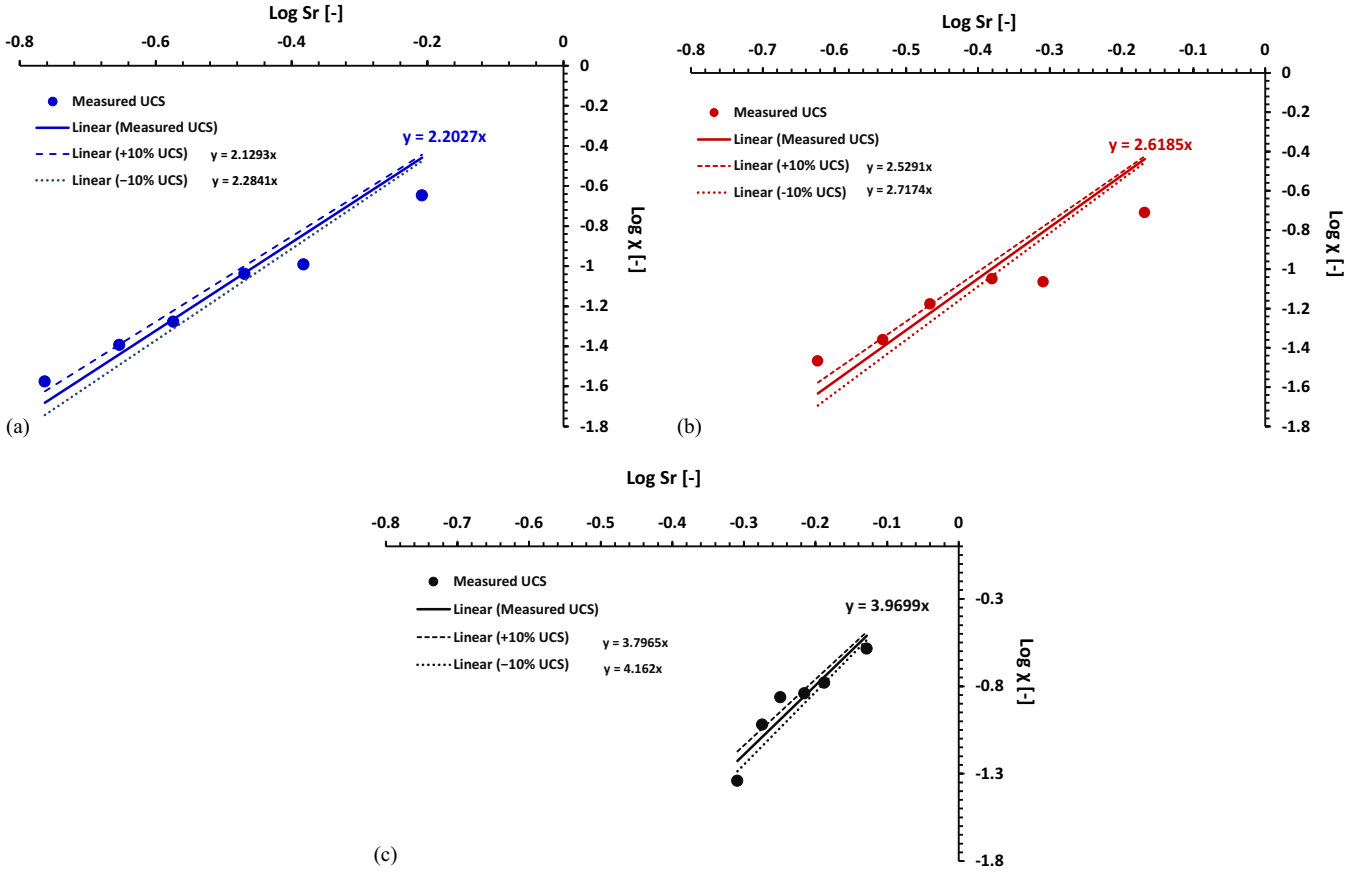

Fig. 11. Calibration of the α exponent as the slope of the linear regression curve in the ($\log S_r$;$\log\chi$) plane: (a) Soignies soil; (b) Kruibeke soil; and (c) Tournai soil. Sensitivity of χ calibration to $\alpha \pm \alpha 10\%$ variation in UCS for the tested soils. Solid, dashed, and dotted lines represent the measured UCS, +10% UCS, and −10% UCS cases, respectively.

pores not intruded by mercury during MIP. Instead of porosities, it is more convenient to work with void ratios because the void space is reported with respect to a constant value (i.e., the volume of solid particles), in opposition to porosity, which is reported to a changing parameter (i.e., the total volume). In addition to porosities, Table 6 reports also the total, micro-, and macrovoid ratios.

Then, during the application of suction, the observed shrinkage is considered to result entirely from the reduction of the macrovoid

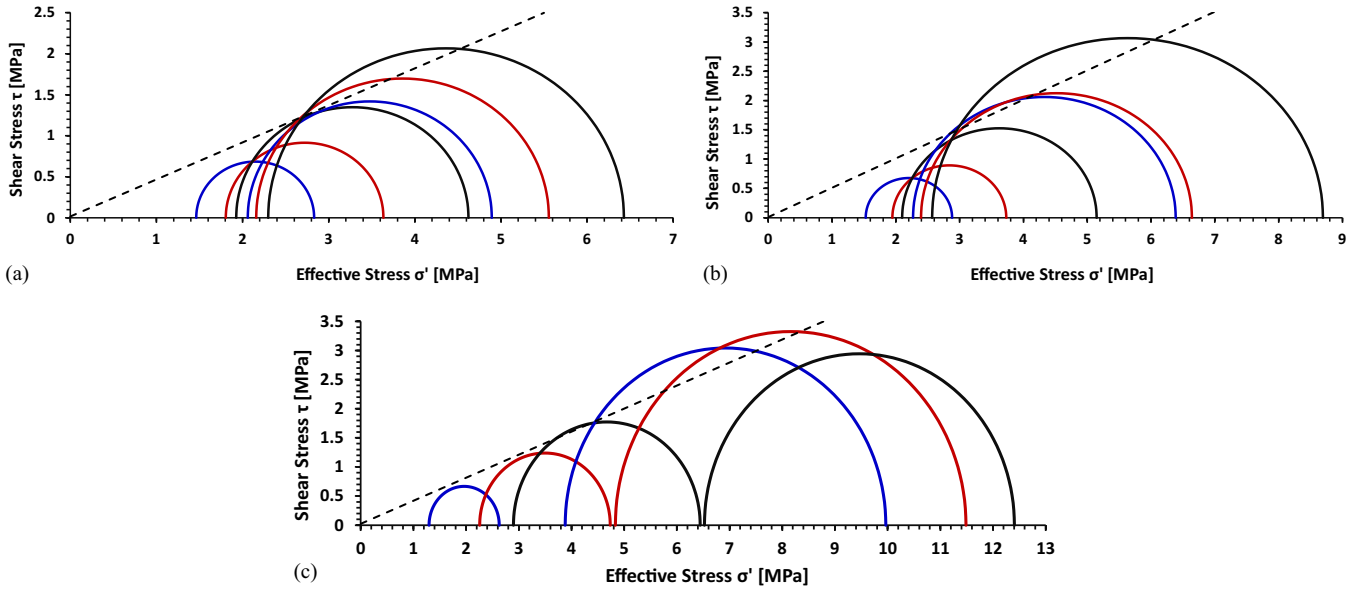

Fig. 12. Mohr circles at failure expressed in terms of generalized effective stress for uniaxial compression tests performed at different suctions: (a) Soignies soil; (b) Kruibeke soil; and (c) Tournai soil.

Downloaded from ascelibrary.org by Bertrand FRANCOIS on 05/02/26. Copyright ASCE. For personal use only; all rights reserved.

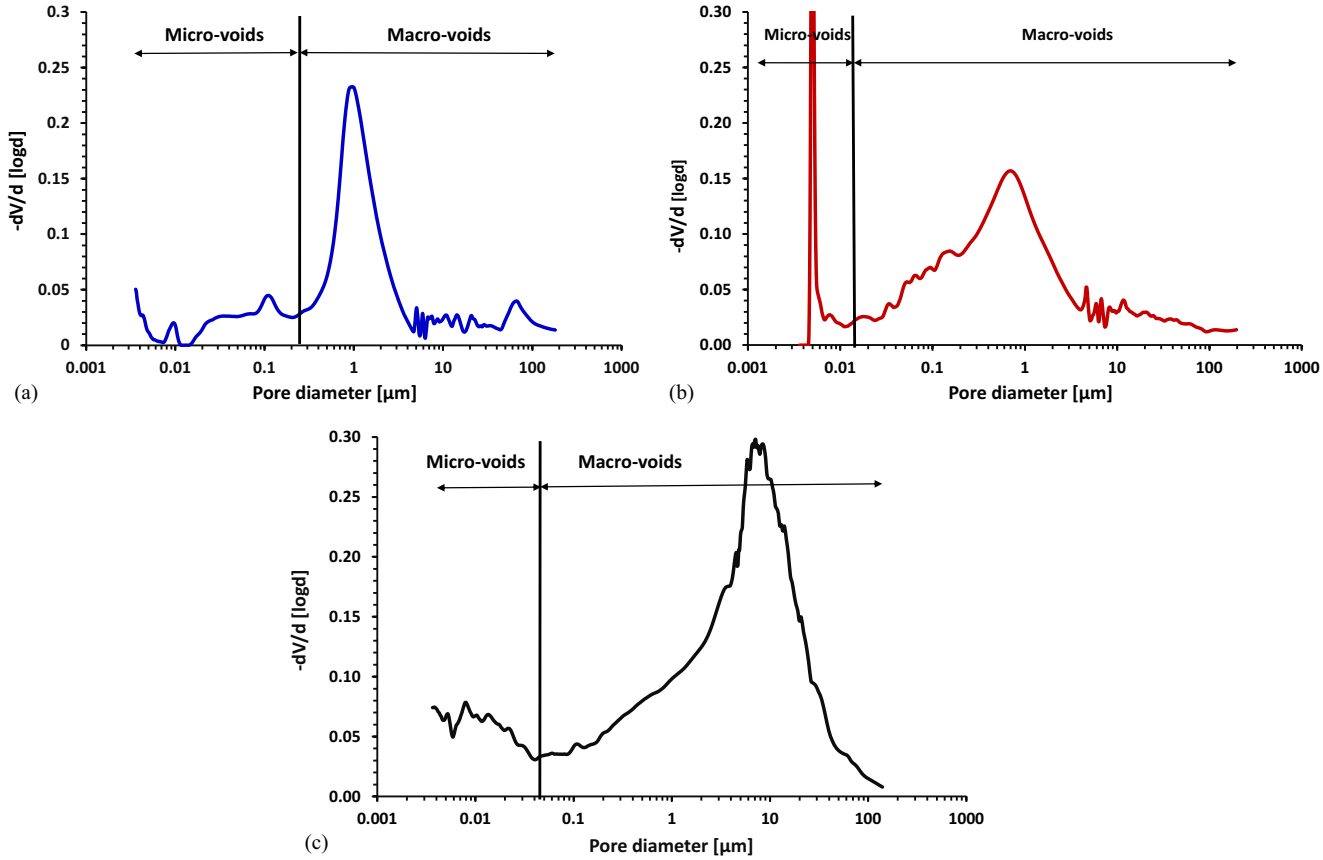

Fig. 13. PSD of the three soils obtained from MIP; differentiation between micro- and macrovoids is delimited by the lowest point of the PSD at intermediate pore diameter: (a) Soignies soil; (b) Kruibeke soil; and (c) Tournai soil.

ratio. Within this framework, the aggregates, comprising the microvoids, are regarded as incompressible, and the closure of the macrovoids accounts for the overall macroscopic shrinkage. Consequently, as drying progresses, the volume of macrovoids decreases, whereas the microvoids remain unchanged. Fig. 14 reports the evolution of total, micro-, and macrovoid ratios, based on the volumetric strain as a function of suction, as reported in Fig. 8.

Once the total, micro-, and macrovoid ratios are determined at different suction levels, the χ parameter can be inferred based on the concept presented in Eq. (2). Fig. 15 illustrates how χ varies with the degree of saturation for the three tested soils, as obtained through four distinct interpretative approaches:

1. The χ value for which the shear failures observed in uniaxial compression tests conducted at different suction levels coincide with the failure envelope established under saturated conditions.
2. The power–law relationship expressed in Eq. (3), where the α exponent is calibrated following the procedure described in the "Methodology for χ Parameter Calibration" section.
3. Eq. (2), which assumes that the void ratio remains unchanged throughout the drying process (i.e., $S_r^m = S_{r,0}^m = \text{constant}$).
4. Eq. (2), which accounts for the evolution of void ratio during drying as illustrated in Fig. 14, where the overall decrease in void ratio is entirely attributed to the reduction of macrovoids (i.e., S_r^m increases upon drying).

Table 6. Microstructural parameters of the three soils as deduced from mercury intrusion porosimetry

Soil	Soignies	Kruibeke	Tournai
Intruded porosity	0.327	0.395	0.472
Intruded microporosity	0.060	0.044	0.069
Intruded macroporosity	0.267	0.351	0.402
Total porosity	0.346	0.483	0.587
Total microporosity	0.079	0.132	0.185
Total macroporosity	0.267	0.351	0.402
Total void ratio	0.529	0.934	1.421
Total microvoid ratio	0.121	0.256	0.447
Total macrovoid ratio	0.408	0.678	0.974
Initial microstructural degree of saturation $S_{r,0}^m$	0.314	0.274	0.229

When the χ parameter is obtained experimentally from uniaxial compression tests at various suctions to fulfill a unique failure criterion (Approach 1), the relation between χ and S_r shows reasonable consistency with the microstructural conceptual model proposed by Tarantino and Tombolato (2005). The χ parameter remains insignificant at low degrees of saturation, in which water is mainly confined within the intra-aggregate micropores. The power–law relationship (Approach 2) provides a satisfactory fit to the experimental χ values for the Tournai soil, which exhibits the highest plasticity among the tested materials. However, for Kruibeke and Soignies soils, the matching is less good for the lower suction levels (i.e., the higher degree of saturation). But still, the trend of the curve agrees with the experimental points. For Approach 3, which disregards microstructural evolution during drying, the transition between dry and water-filled macrovoids appears overly abrupt. In practice, this transition is more gradual, as water progressively infiltrates the macrovoids even before the microvoids become completely saturated. Moreover, assuming an invariant microstructure during drying is a restrictive hypothesis, as it tends to underestimate the S_r^m values at high suction levels. In fact, at elevated suctions, shrinkage considerably reduces the

Downloaded from ascelibrary.org by Bertrand FRANCOIS on 05/02/26. Copyright ASCE. For personal use only; all rights reserved.

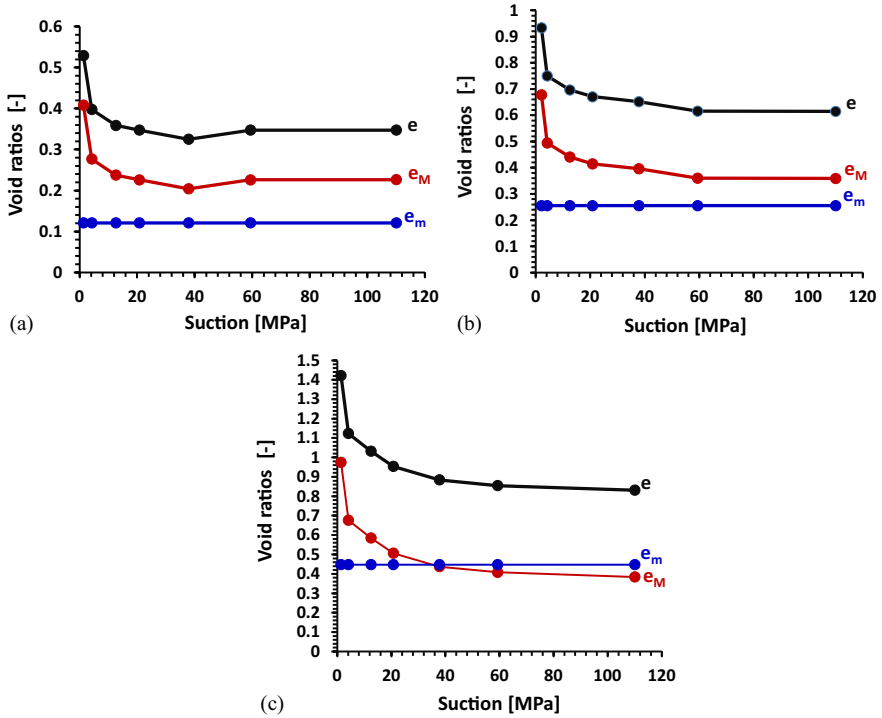

Fig. 14. Evolution of total void ratio (e), macrovoid ratio (e_M), and microvoid ratio (e_m) during drying, assuming that the microvoid ratio (intra-aggregate) remains constant: (a) Soignies soil; (b) Kruibeke soil; and (c) Tournai soil.

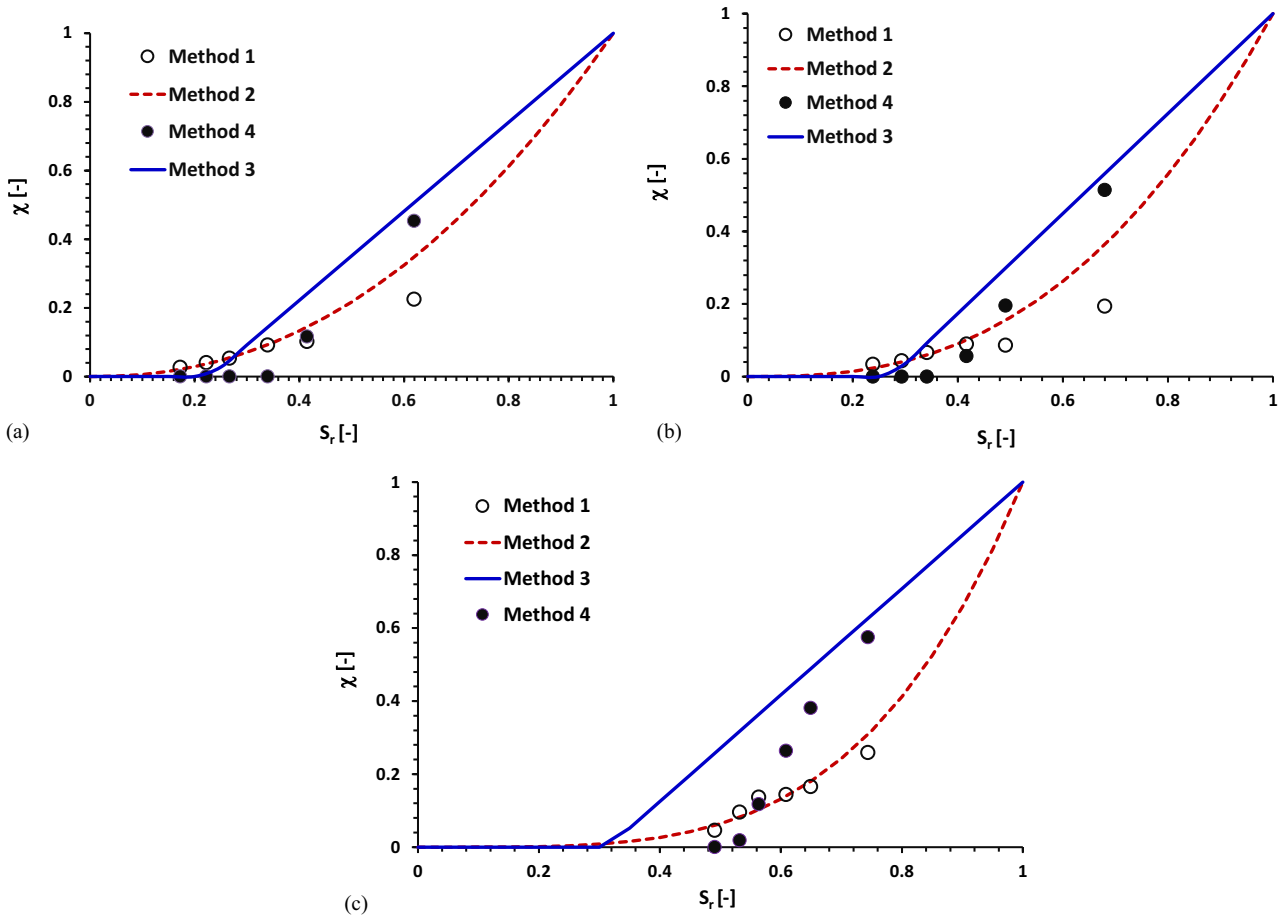

Fig. 15. χ parameter as a function of the degree of saturation of the (a) Soignies soil; (b) Kruibeke soil; and (c) Tournai soil according to four different approaches: (1) from uniaxial compression strength at various suctions; (2) fitting through a power law of the point obtained by Approach 1; (3) from Eq. (2) assuming the void ratio remains constant upon drying; and (4) from Eq. (2) with varying macrovoid ratio upon drying.

Downloaded from ascelibrary.org by Bertrand FRANCOIS on 05/02/26. Copyright ASCE. For personal use only; all rights reserved.

macrovoids, resulting in a higher proportion of microvoids relative to the total pore volume. Finally, Approach 4 provides a more realistic overall trend compared to Approach 3, although the transition between dry and water-invaded macrovoids remains somewhat abrupt for the same underlying reason associated with Approach 3 (i.e., water starts to invade macrovoids before full saturation of microvoids).

Conclusion

Applying a generalized effective stress framework to unsaturated soils necessitates calibrating the effective stress parameter, known as the χ parameter. In this research, χ is formulated as a power–law function of the degree of saturation. The calibration approach involved conducting triaxial compression tests under saturated conditions to establish the intrinsic (effective) shear failure criterion, defined by the effective cohesion and friction angle. Subsequently, a series of uniaxial compression tests at different suctions (corresponding to various degrees of saturation) were performed to determine one χ value per saturation level, allowing the uniaxial compression strengths to align with the intrinsic failure criterion expressed in terms of effective stress. Ultimately, the power–law relationship was fitted to best represent the correlation between χ and the degree of saturation.

The exponent in the power law dictates how rapidly χ increases with the degree of saturation. At low saturation levels, in which water resides primarily within the micropores, χ remains negligible because this intra-aggregate water does not contribute to the macroscopic stress. Conversely, at higher saturation levels, water begins to occupy the interaggregate voids, thereby playing a more substantial role in the increase of the effective stress (i.e., χ becomes significant).

To investigate the microstructural perspective, pore size distributions obtained from mercury intrusion porosimetry were analyzed considering their bimodal character. When the degree of saturation remains below the microstructural degree of saturation the χ parameter is negligible while when the degree of saturation overpasses the microstructural degree of saturation, water invades the macroporosity and the χ parameter increases more significantly.

This method has been applied to three compacted clayey soils with different plasticity indexes. The soil with the highest plasticity index develops the highest cohesion, the lowest friction angle, the highest retention capacity, and the highest shrinkage upon drying. Also, the most plastic soil demonstrates the highest exponent of the power law.

At the end, the proposed methodology provides a simple but efficient and comprehensive protocol to calibrate the χ parameter, based on the assumption that the shear failure criterion remains unique when represented in terms of generalized effective stress.

Appendix. Effective Stress Parameters Expressed as Functions of Degree of Saturation or Suction and Associated Microstructural Features

Expressions of χ parameter	Reference	Explanation
$\chi = \begin{cases} \left(\frac{s}{s_e}\right)^{-0.55} & \text{if } s > s_e \\ 1 & \text{if } s \le s_e \end{cases}$	Khalili and Khabbaz (1998)	s_e: air-entry suction
$\chi = S_r$	Schrefler (1984)	—
$\chi = \frac{S_r - S_{r0}}{1 - S_{r0}}$	Kim et al. (2010)	S_{r0}: the residual degree of saturation
$\chi = \frac{S_r - S_r^m}{1 - S_r^m} + \frac{1}{n_{\text{smooth}}} \ln\left[1 + \exp\left(-n_{\text{smooth}} \frac{S_r - S_r^m}{1 - S_r^m}\right)\right]$	Alonso et al. (2013)	S_r^m : microstructural degree of saturation[a] n_{smooth} defines the degree of smoothing of the function $\chi(S_r)$
$\chi = S_{rM} + (e - e_{wm}) \frac{\delta S_{rM}}{\delta(e - e_{wm})}\Big\|_{s=cst}$ with $S_{rM} = \frac{e_w - e_{wm}}{e - e_{wm}}$	Vaunat and Casini (2017)	e: void ratio $e_w = \frac{V_w}{V_s}$: water ratio $e_{wm} = \frac{V_{wm}}{V_s}$: microstructural water ratio[b]
$\chi = \left\langle \frac{S_r - S_r^m}{1 - S_r^m} \right\rangle$	Alonso et al. (2010)	S_r^m : microstructural degree of saturation[a]
$\chi = (S_r)^{\alpha}$	Alonso et al. (2010)	α: material parameter
$\chi = \begin{cases} \frac{e_w - e_{wm}}{e - e_{wm}} = \frac{S_r - S_r^m}{1 - S_r^m} & \text{if } S_r > S_r^m \\ 0 & \text{if } S_r > S_r^m \end{cases}$	Tarantino and Tombolato (2005)	S_r^m : microstructural degree of saturation[a]
$\chi = \frac{S_r - S_{r0}}{1 - S_{r0}} + \frac{k^{aw} a_{aw}}{s}$	Nikooee et al. (2013)	a_{aw}: specific air–water interfacial area, defined as the ratio of the air–water interface area to the total volume k^{aw}: a material constant associated with the air–water surface tension
$\chi = (1 - n) x_{sw} + n S_r$	Gray et al. (2009)	x_{sw}: the fraction of wetted solid surface area n : porosity
$\chi = S_r^{(\beta_1 / S_r^{\beta_2})}$	Ghorbani and Kodikara (2024)	β_1, β_2: material parameters
$\chi = \begin{cases} s_e + \frac{(s_c - s_e)(s - s_e)}{(s - s_e) + a_e} & \text{if } s > s_e \\ 1 & \text{if } s \le s_e \end{cases}$	Kohgo et al. (1993)	a_e: material parameter s_c: a critical suction s_e: air-entry suction

[a]Microstructural degree of saturation: Degree of saturation required to saturate microvoids and let macrovoids empty.
[b]Microstructural water ratio: Water ratio required to saturate microvoids and let macrovoids empty.

Int. J. Geomech., 2026, 26(7): 04026118

Downloaded from ascelibrary.org by Bertrand FRANCOIS on 05/02/26. Copyright ASCE. For personal use only; all rights reserved.

Data Availability Statement

Data sets generated during the current study are available from the corresponding author upon reasonable request.

Author Contributions

Hesam Ebrahimisadr: Investigation, Methodology, Validation, Writing—original draft; Sophie Lanckohr: Formal analysis, Investigation; Bertrand François: Conceptualization, Funding acquisition, Methodology, Validation, Visualization, Writing—review and editing.

References

Alonso, E. E., J.-M. Pereira, J. Vaunat, and S. Olivella. 2010. "A microstructurally based effective stress for unsaturated soils." *Géotechnique* 60 (12): 913–925. https://doi.org/10.1680/geot.8.P.002.

Alonso, E. E., N. M. Pinyol, and A. Gens. 2013. "Compacted soil behaviour: Initial state, structure and constitutive modelling." *Géotechnique* 63 (6): 463–478. https://doi.org/10.1680/geot.11.P.134.

Arlabosse, P., E. Rodier, J. H. Ferrasse, S. Chavez, and D. Lecomte. 2003. "Comparison between static and dynamic methods for sorption isotherm measurements." *Drying Technol.* 21 (3): 479–497. https://doi.org/10.1081/DRT-120018458.

ASTM. 2010. *Standard test method for measurement of soil potential (suction) using filter paper*. ASTM D5298-10. West Conshohocken, PA: ASTM.

Bishop, A. W. 1959. "The principle of effective stress." *Teknisk Ukeblad* 39: 859–863.

Bishop, A. W., I. Alpan, G. E. Blight, and I. B. Donald. 1960. "Factors controlling the strength of partly saturated cohesive soils." In *Proc., Research Conf. on Shear Strength of Cohesive Soils* 503–532. Reston, VA: ASCE.

Cao, T. D., and L. Sun. 2025. "Temperature-dependent elastoplastic behavior of low plasticity unsaturated soils." *Acta Geotech.* 20: 2889–2909. https://doi.org/10.1007/s11440-025-02554-6.

Delage, P., M. D. Howat, and Y. J. Cui. 1998. "The relationship between suction and swelling properties in a heavily compacted unsaturated clay." *Eng. Geol.* 50 (1–2): 31–48. https://doi.org/10.1016/S0013-7952(97)00083-5.

Ebrahimisadr, H., S. Lanckohr, and B. Francois. 2025. "A methodology for the calibration of the effective stress parameter: From macroscopic considerations to microstructural validation." *E3S Web Conf.* 642: 02003. https://doi.org/10.1051/e3sconf/202564202003.

Gallipoli, D., P. Grassl, S. Wheeler, and A. Gens. 2018. "On the choice of stress–strain variables for unsaturated soils and its effect on plastic flow." *Geomech. Energy Environ.* 15: 3–9. https://doi.org/10.1016/j.gete.2018.02.002.

Gallipoli, D., S. J. Wheeler, and M. Karstunen. 2003. "Modelling the variation of degree of saturation in a deformable unsaturated soil." *Géotechnique* 53 (1): 105–112. https://doi.org/10.1680/geot.53.1.105.37249.

Gens, A., M. Sánchez, and D. Sheng. 2006. "On constitutive modelling of unsaturated soils." *Acta Geotech.* 1 (3): 137–147. https://doi.org/10.1007/s11440-006-0013-9.

Gerard, P., M. Mahdad, A. R. McCormack, and B. François. 2015. "A unified failure criterion for unstabilized rammed earth materials upon varying relative humidity conditions." *Constr. Build. Mater.* 95: 437–447. https://doi.org/10.1016/j.conbuildmat.2015.07.100.

Ghorbani, J., and J. Kodikara. 2024. "Thermodynamically consistent effective stress formulation for unsaturated soils across a wide range of soil saturation." *Comput. Mech.* 73 (5): 1077–1094. https://doi.org/10.1007/s00466-023-02401-z.

Gray, W. G., B. A. Schrefler, and F. Pesavento. 2009. "The solid phase stress tensor in porous media mechanics and the Hill–Mandel condition." *J. Mech. Phys. Solids* 57 (3): 539–554. https://doi.org/10.1016/j.jmps.2008.11.005.

Haeri, S. M., S. S. Borujerdi, and A. A. Garakani. 2023. "Effects of initial shear stress on the hydromechanical behavior of collapsible soils." *Acta Geotech.* 18 (11): 6051–6076. https://doi.org/10.1007/s11440-023-02034-9.

Haeri, S. M., A. A. Garakani, A. Khosravi, and C. L. Meehan. 2014. "Assessing the hydro-mechanical behavior of collapsible soils using a modified triaxial test device." *Geotech. Test. J.* 37 (2): 190–204. https://doi.org/10.1520/GTJ20130034.

Haeri, S. M., A. Khosravi, A. A. Garakani, and S. Ghazizadeh. 2017. "Effect of soil structure and disturbance on hydromechanical behavior of collapsible loessial soils." *Int. J. Geomech.* 17 (1): 04016021. https://doi.org/10.1061/(ASCE)GM.1943-5622.0000656.

Jennings, J. E. B., and J. B. Burland. 1962. "Limitations to the use of effective stresses in partly saturated soils." *Géotechnique* 12 (2): 125–144. https://doi.org/10.1680/geot.1962.12.2.125.

Khalili, N., and M. H. Khabbaz. 1998. "A unique relationship for χ for the determination of the shear strength of unsaturated soils." *Géotechnique* 48 (5): 681–687. https://doi.org/10.1680/geot.1998.48.5.681.

Khalili, N., R. Witt, L. Laloui, L. Vulliet, and A. Koliji. 2005. "Effective stress in double porous media with two immiscible fluids." *Geophys. Res. Lett.* 32 (15): L15309. https://doi.org/10.1029/2005GL023766.

Khoshghalb, A., and B. Shahbodagh. 2025. "Discussion of 'Indefinability of effective stress for unsaturated soils'." *J. Geotech. Geoenviron. Eng.* 151 (9): 07025010. https://doi.org/10.1061/JGGEFK.GTENG-13624.

Kim, B.-S., S. Shibuya, S.-W. Park, and S. Kato. 2010. "Application of suction stress for estimating unsaturated shear strength of soils using direct shear testing under low confining pressure." *Can. Geotech. J.* 47 (9): 955–970. https://doi.org/10.1139/T10-007.

Kohgo, Y., M. Nakano, and T. Miyazaki. 1993. "Theoretical aspects of constitutive modelling for unsaturated soils." *Soils Found.* 33 (4): 49–63. https://doi.org/10.3208/sandf1972.33.4_49.

Likos, W. J. 2014. "Effective stress in unsaturated soil: Accounting for surface tension and interfacial area." *Vadose Zone J.* 13 (5): 1–12. https://doi.org/10.2136/vzj2013.05.0095.

Lu, N., J. W. Godt, and D. T. Wu. 2010. "A closed-form equation for effective stress in unsaturated soil." *Water Resour. Res.* 46 (5): W05515. https://doi.org/10.1029/2009wr008646.

Lu, N., and D. V. Griffiths. 2004. "Profiles of steady-state suction stress in unsaturated soils." *J. Geotech. Geoenviron. Eng.* 130 (10): 1063–1076. https://doi.org/10.1061/(ASCE)1090-0241(2004)130:10(1063).

Lu, N., and W. J. Likos. 2006. "Suction stress characteristic curve for unsaturated soil." *J. Geotech. Geoenviron. Eng.* 132 (2): 131–142. https://doi.org/10.1061/(ASCE)1090-0241(2006)132:2(131).

Mohyla, T., J. Boháč, and D. Mašín. 2021. "Small-strain behaviour of unsaturated silty clay: Experiments and model interpretation." *Acta Geotech.* 16 (9): 2837–2849. https://doi.org/10.1007/s11440-021-01204-x.

Morvan, M., and D. Perić. 2025. "Discussion of 'Indefinability of effective stress for unsaturated soils'." *J. Geotech. Geoenviron. Eng.* 151 (9): 07025011. https://doi.org/10.1061/JGGEFK.GTENG-13629.

Nikooee, E., G. Habibagahi, S. M. Hassanizadeh, and A. Ghahramani. 2013. "Effective stress in unsaturated soils: A thermodynamic approach based on the interfacial energy and hydromechanical coupling." *Transp. Porous Media* 96 (2): 369–396. https://doi.org/10.1007/s11242-012-0093-y.

Nuth, M., and L. Laloui. 2008. "Effective stress concept in unsaturated soils: Clarification and validation of a unified framework." *Int. J. Numer. Anal. Methods Geomech.* 32 (7): 771–801. https://doi.org/10.1002/nag.645.

Öberg, A. L., and G. Sällfors. 1997. "Determination of shear strength parameters of unsaturated silts and sands based on the water retention curve." *Geotech. Test. J.* 20 (1): 40–48. https://doi.org/10.1520/GTJ11419J.

Pham, T. A. 2022. "Micromechanical-based shear strength equation considering the stress-state effect for unsaturated soils." *Int. J. Geomech.* 22 (9): 06022022. https://doi.org/10.1061/(ASCE)GM.1943-5622.0002495.

Downloaded from ascelibrary.org by Bertrand FRANCOIS on 05/02/26. Copyright ASCE. For personal use only; all rights reserved.

Rojas, E. 2025. "Discussion of 'Indefinability of effective stress for unsaturated soils'." *J. Geotech. Geoenviron. Eng.* 151 (9): 07025012. https://doi.org/10.1061/JGGEFK.GTENG-13630.

Schmitz, R. M., C. Schroeder, and R. Charlier. 2004. "Chemo–mechanical interactions in clay: A correlation between clay mineralogy and Atterberg limits." *Appl. Clay Sci.* 26 (1–4): 351–358. https://doi.org/10.1016/j.clay.2003.12.015.

Schrefler, B. A. 1984. "The finite element method in soil consolidation (with applications to surface subsidence)." Ph.D. thesis, Dept. of Civil Engineering, Univ. College of Swansea.

Tarantino, A., and G. El Mountassir. 2013. "Making unsaturated soil mechanics accessible for engineers: Preliminary hydraulic–mechanical characterisation & stability assessment." *Eng. Geol.* 165: 89–104. https://doi.org/10.1016/j.enggeo.2013.05.025.

Tarantino, A., and S. Tombolato. 2005. "Coupling of hydraulic and mechanical behaviour in unsaturated compacted clay." *Géotechnique* 55 (4): 307–317. https://doi.org/10.1680/geot.2005.55.4.307.

Terzaghi, K. 1936. *Theoretical soil mechanics*. New York: Wiley.

Vanapalli, S. K., and D. G. Fredlund. 2000. "Comparison of different procedures to predict unsaturated soil shear strength." In *Advances in Unsaturated Geotechnics*, Geotechnical Special Publication 99, edited by C. D. Shackelford, S. L. Houston, and N.-Y. Chang, 195–209. Reston, VA: ASCE.

van Genuchten, M. T. 1980. "A closed-form equation for predicting the hydraulic conductivity of unsaturated soils." *Soil Sci. Soc. Am. J.* 44 (5): 892–898. https://doi.org/10.2136/sssaj1980.03615995004400050002x.

Vaunat, J., and F. Casini. 2017. "A poromechanical framework to model soil fabric evolution and its effect on material hydromechanical response." In *Proc., 6th Biot Conf. on Poromechanics*, 1443–1450. Reston, VA: ASCE.

Wang, J., D. Zhang, N. Wang, and T. Gu. 2019. "Mechanisms of wetting-induced loess slope failures." *Landslides* 16 (5): 937–953. https://doi.org/10.1007/s10346-019-01144-4.

Zhan, T. L. T., R. Chen, and C. W. W. Ng. 2014. "Wetting-induced softening behavior of an unsaturated expansive clay." *Landslides* 11 (6): 1051–1061. https://doi.org/10.1007/s10346-013-0449-6.

Zhang, C., and N. Lu. 2018. "What is the range of soil water density? Critical reviews with a unified model." *Rev. Geophys.* 56 (3): 532–562. https://doi.org/10.1029/2018RG000597.

Zhang, C., and N. Lu. 2019. "Unitary definition of matric suction." *J. Geotech. Geoenviron. Eng.* 145 (2): 02818004. https://doi.org/10.1061/(ASCE)GT.1943-5606.0002004.

Zhang, C., and N. Lu. 2020. "Unified effective stress equation for soil." *J. Eng. Mech.* 146 (2): 04019135. https://doi.org/10.1061/(ASCE)EM.1943-7889.0001718.

Zhang, X., and S. Houston. 2024. "Indefinability of effective stress for unsaturated soils." *J. Geotech. Geoenviron. Eng.* 150 (8): 04024064. https://doi.org/10.1061/JGGEFK.GTENG-12435.

Zhang, X., and S. Houston. 2025. "Closure to 'Indefinability of effective stress for unsaturated soils'." *J. Geotech. Geoenviron. Eng.* 151 (9): 07025013. https://doi.org/10.1061/JGGEFK.GTENG-13965.

Zhou, Y. F., L. G. Tham, W. M. Yan, F. C. Dai, and L. Xu. 2014. "Laboratory study on soil behavior in loess slope subjected to infiltration." *Eng. Geol.* 183: 31–38. https://doi.org/10.1016/j.enggeo.2014.09.010.

Downloaded from ascelibrary.org by Bertrand FRANCOIS on 05/02/26. Copyright ASCE. For personal use only; all rights reserved.